Metal Nanowire Felt as a Flow-Through Electrode for High-Productivity Electrochemistry

Myung Jun Kim,[1] Youngran Seo,[2] Mutya A. Cruz,[1] and Benjamin J. Wiley[1*]

[1]Department of Chemistry, Duke University, 124 Science Drive, Box 90354, Durham, North Carolina 27708, United States.

[2]Department of Chemistry, University of North Carolina at Chapel Hill, Chapel Hill, North Carolina 27599, United States.

Table of Contents

Supplementary Text

The Relationship between $k_m A_s$ and u Derived from Dimensionless Numbers

Mass transport of species in the porous electrode as a function of flow rate can be obtained from the relation between Sherwood (*Sh*), Reynolds (*Re*), and Schmidt (*Sc*) numbers,[1–6]

$$Sh = a^* Re^b Sc^c \tag{S1}$$

where a^*, b, and c are real numbers. The equations for *Sh* and *Re* for fibrous porous media vary from study to study (Table S1). The effective diffusion coefficient ($D_{eff} = D \times \varepsilon^{1.5}$) has also been used instead of D.[7] *Sh* and *Re* for fibrous media from previous reports are summarized in Table S1. The type of equation that is used for *Re* and *Sh* will affect the value of the prefactor a in equation (2) in the main text, but not the overall form of the $k_m A_s$ - u relationship. Table S1 shows the prefactor a in equation (2) in the main text is a function of A_s, d, and ε at given D and v.

Supplementary Figures

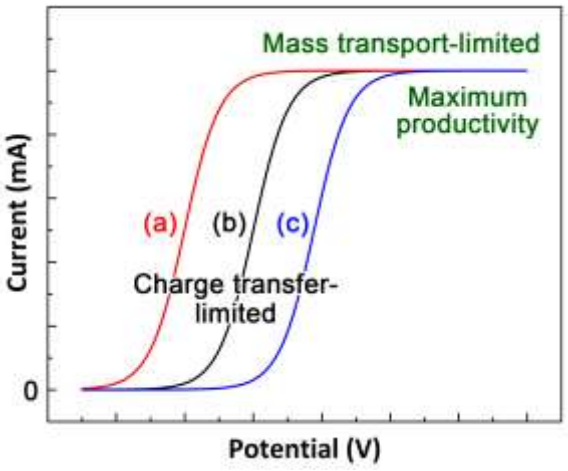

Figure S1. Current-potential curves for three electrode materials with different electrocatalytic activities (a > b > c). The electrode surface area and the mass transport conditions are the same for all electrodes. Although the electrocatalytic activities of the electrodes change the currents in the charge transfer regime, the maximum currents for all electrodes under mass transport-limited conditions are the same, and are therefore not affected by a difference in electrocatalytic activity and electrode potential.

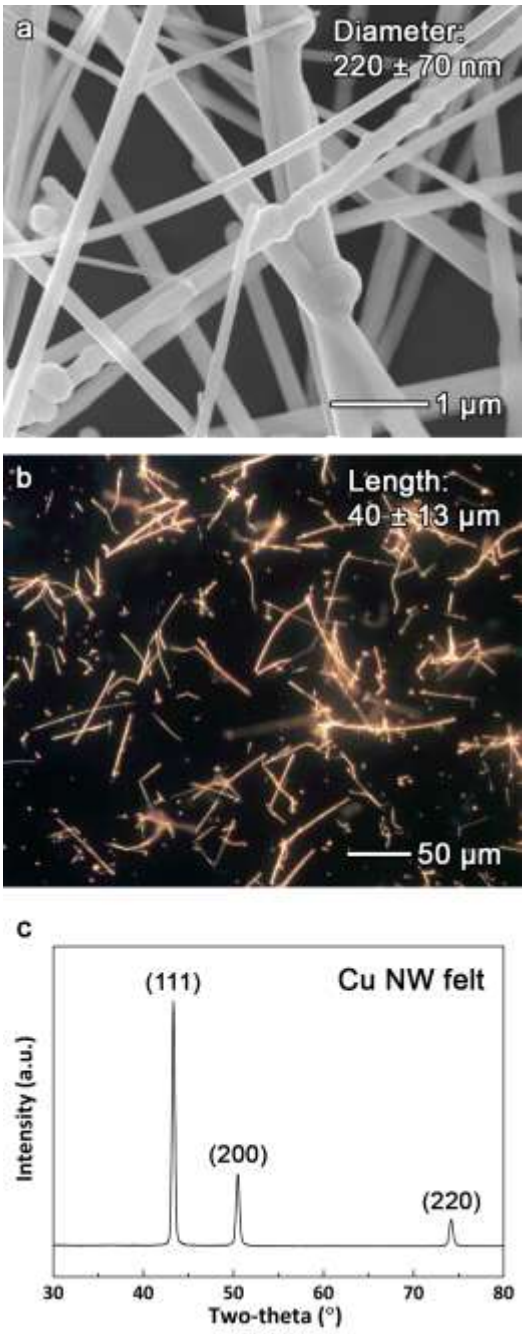

Figure S2. (a) SEM and (b) DFOM images of Cu nanowires used in this study. (c) The XRD pattern for the Cu nanowire felt.

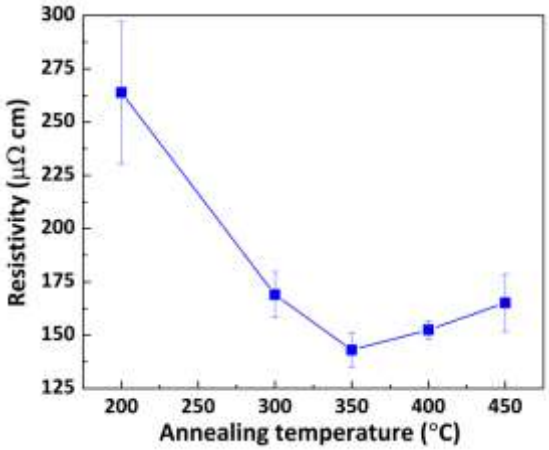

Figure S3. The electrical resistivity of a 324-μm-thick Cu nanowire felt after annealing at various temperatures for 30 min in a H_2 atmosphere.

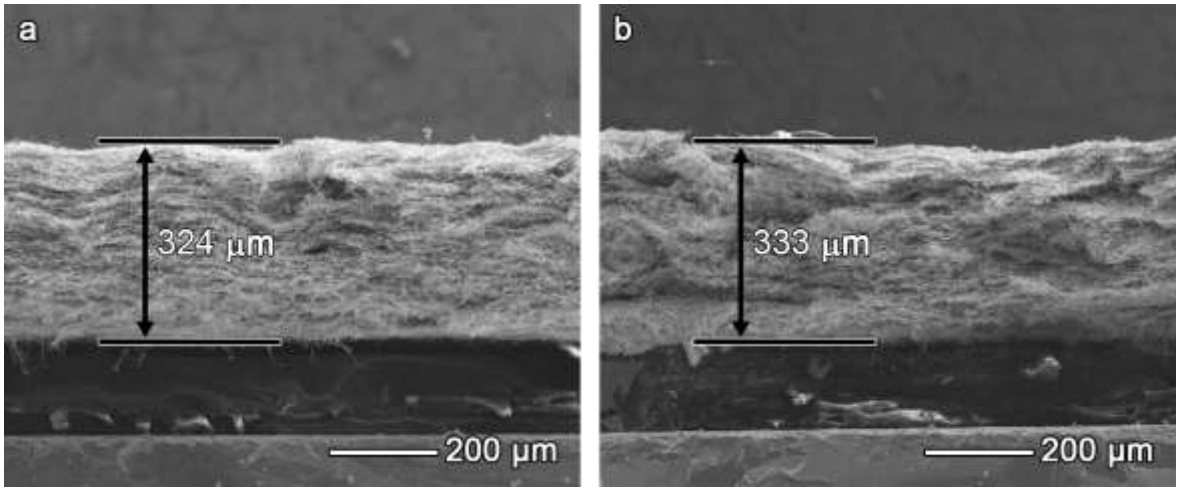

Figure S4. Cross-sectional images of an annealed Cu nanowire felt (a) before and (b) after liquid flow at 1 cm/s for 10 min.

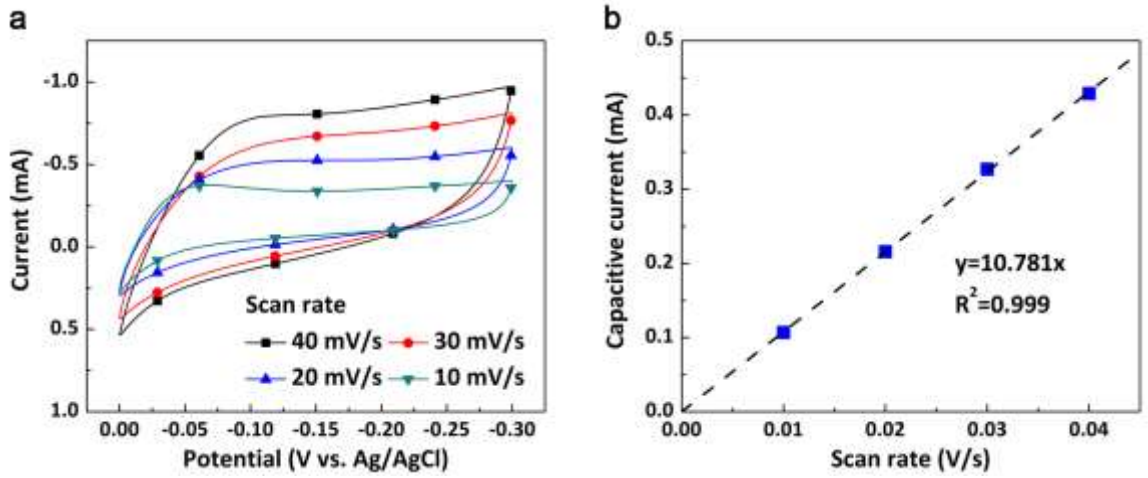

Figure S5. (a) Cyclic voltammograms for Cu nanowire felt in 0.1 M $HClO_4$. (b) The change in the capacitive current with scan rate.

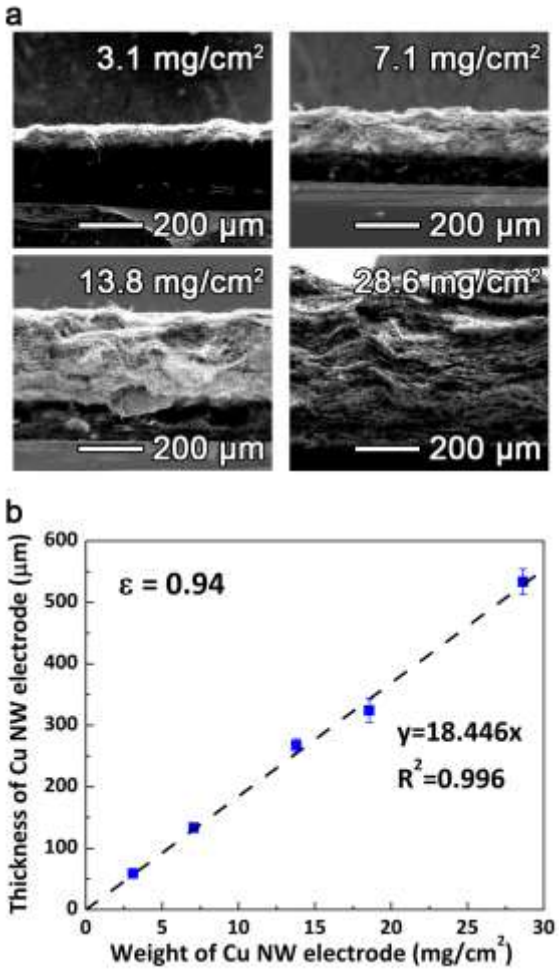

Figure S6. (a) Cross-sectional images of Cu nanowire felts with different thicknesses. (b) The average thickness of electrodes *versus* the weight of Cu nanowires in the felt.

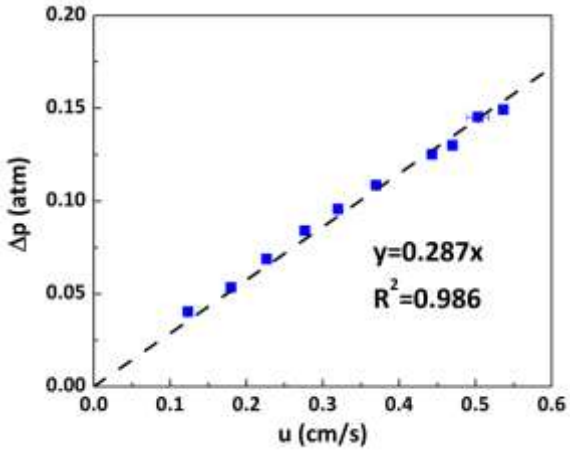

Figure S7. Pressure drop across a 324 μm-thick Cu nanowire felt *versus* superficial flow rate.

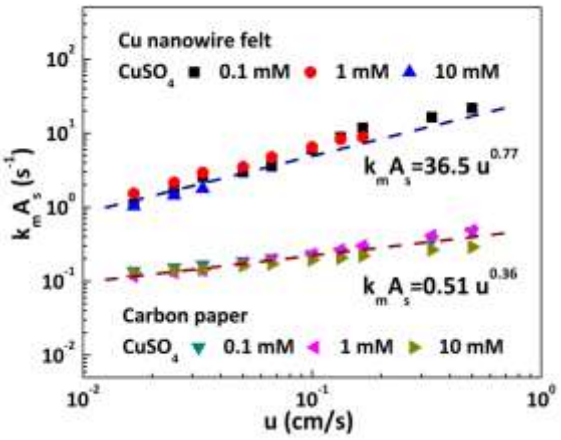

Figure S8. Log-plot for the correlation between $k_m A_s$ and u for the Cu nanowire felt and carbon paper obtained from Figure 3.

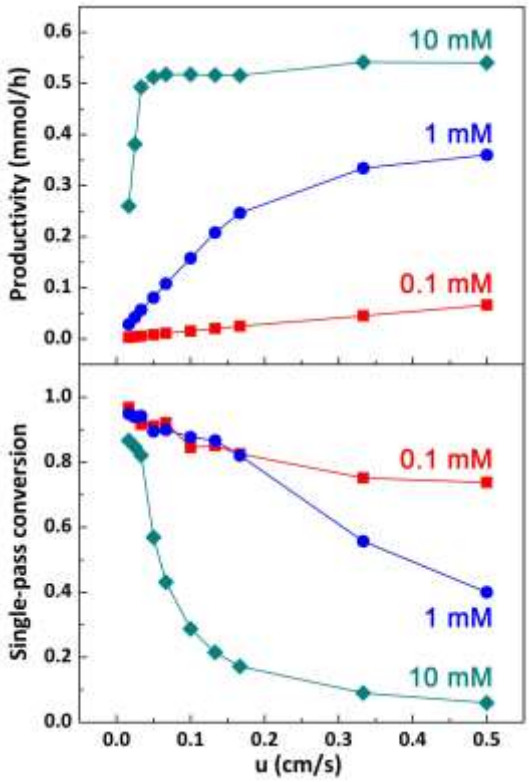

Figure S9. The productivity and single-pass conversion for the reduction of Cu ions with Cu nanowire felts at concentrations of 0.1, 1, and 10 mM as a function of flow rate. The productivity and single-pass conversion were calculated from the current shown in Figure 3.

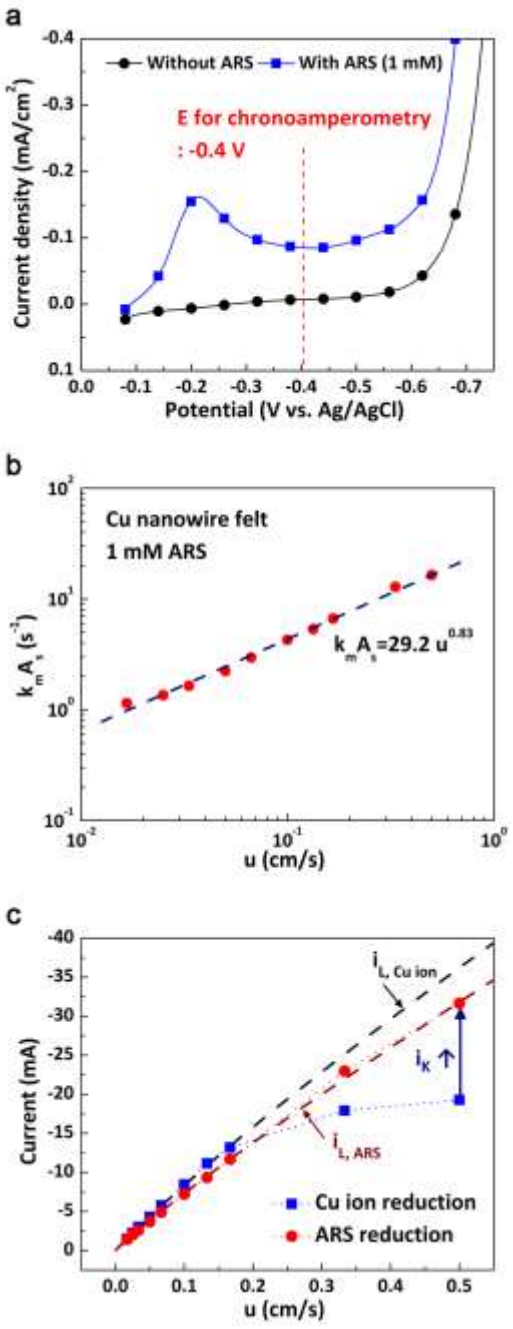

Figure S10. (a) Representative linear sweep voltammogram for ARS reduction on a polycrystalline Cu electrode. (b) The relation of k_mA_s and superficial velocity for ARS reduction with Cu nanowire felt. (c) The average current for the reduction of Cu ions and ARS as a function of superficial velocity.

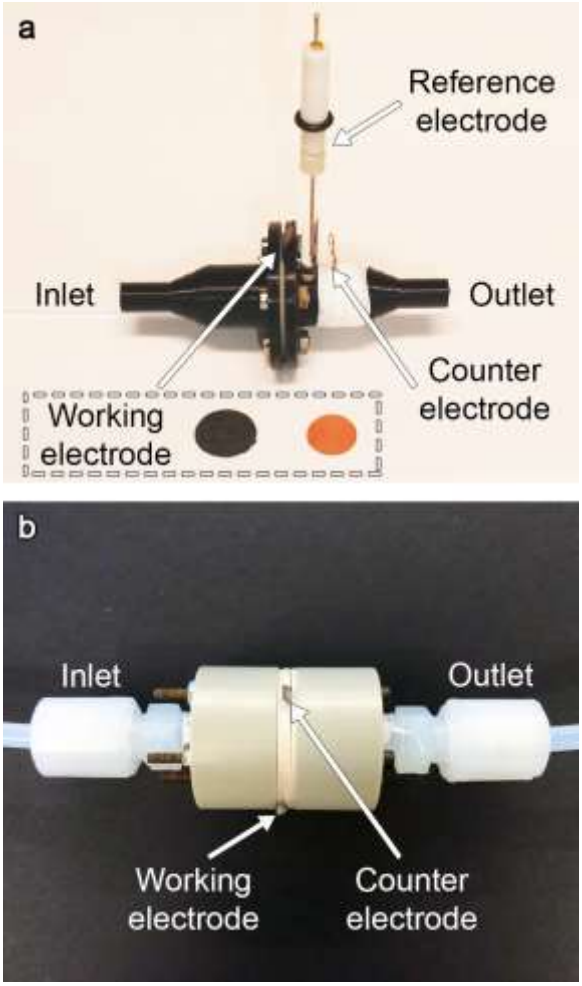

Figure S11. Pictures of (a) a 3D printed flow cell for the reduction of Cu ion and ARS and (b) a PEEK flow cell for electroorganic synthesis.

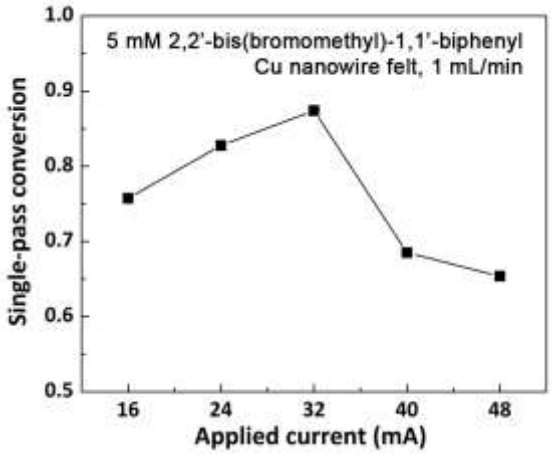

Figure S12. Single pass conversion for the reduction of 2,2′-bis(bromomethyl)-1,1′-biphenyl to 9,10′-dihydrophenanthrene over a Cu nanowire felt as a function of the applied current. The concentration of 2,2′-bis(bromomethyl)-1,1′-biphenyl and the volumetric flow rate were fixed at 5 mM and 1 mL/min, respectively.

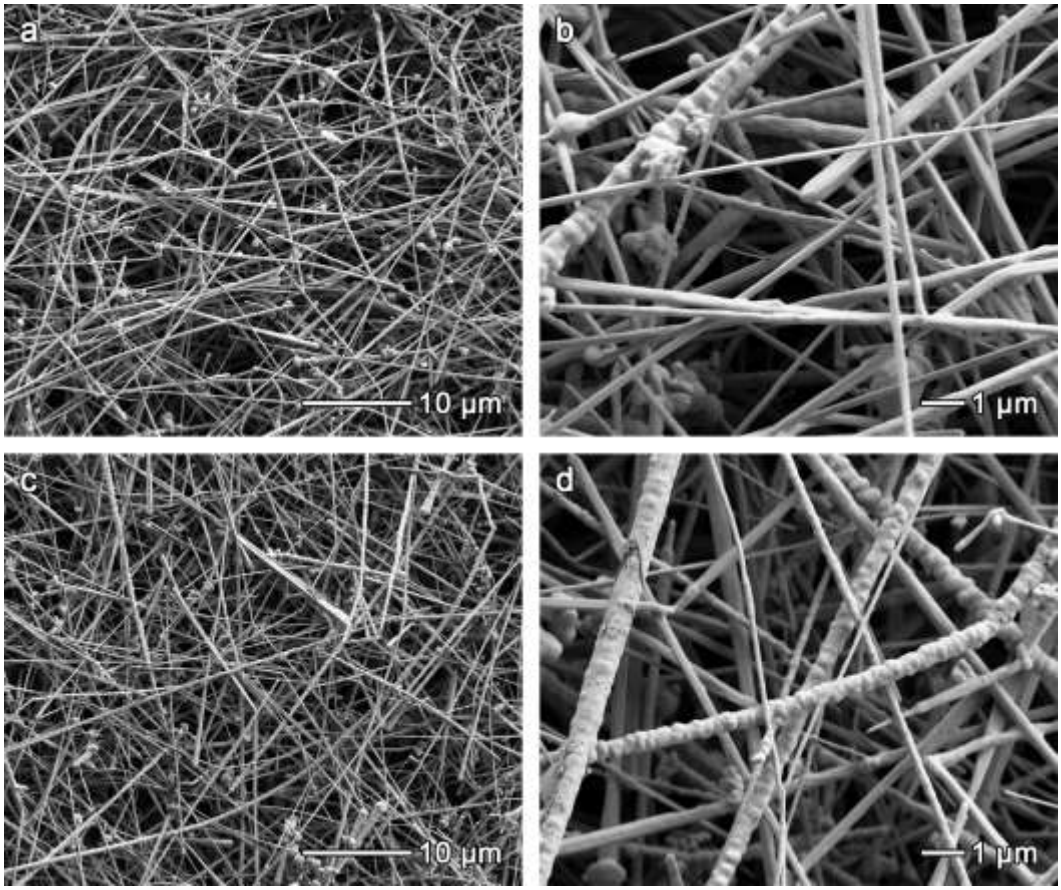

Figure S13. SEM images of Cu nanowire felts (a,b) before and (c,d) after reductive dehalogenation of 2,2′-bis(bromomethyl)-1,1′-biphenyl for 50 min. The flow rate and applied current were 1 mL/min and 32 mA, respectively.

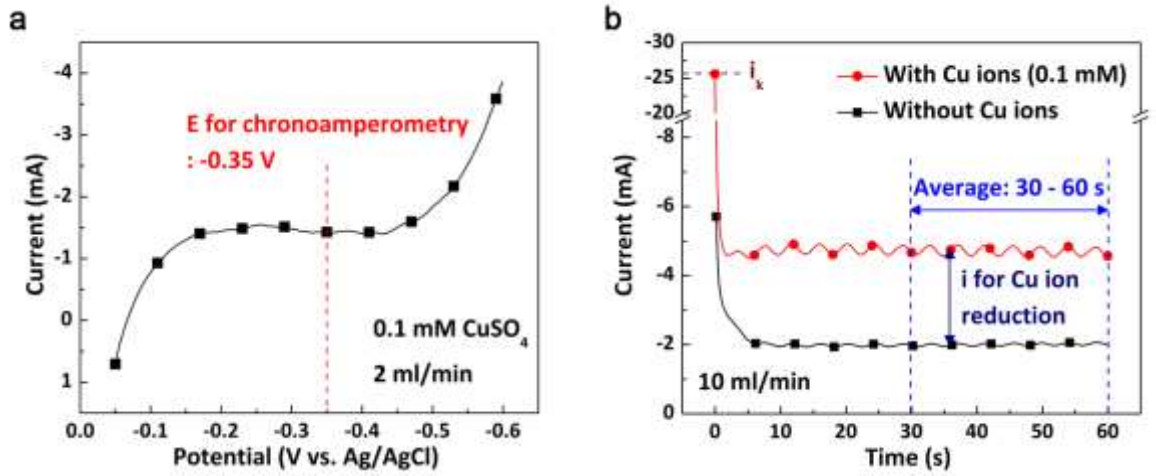

Figure S14. (a) The representative linear sweep voltammogram for Cu ion reduction from Cu nanowire felt. (b) Current-time curves at -0.35 V for electrolytes with and without Cu ions.

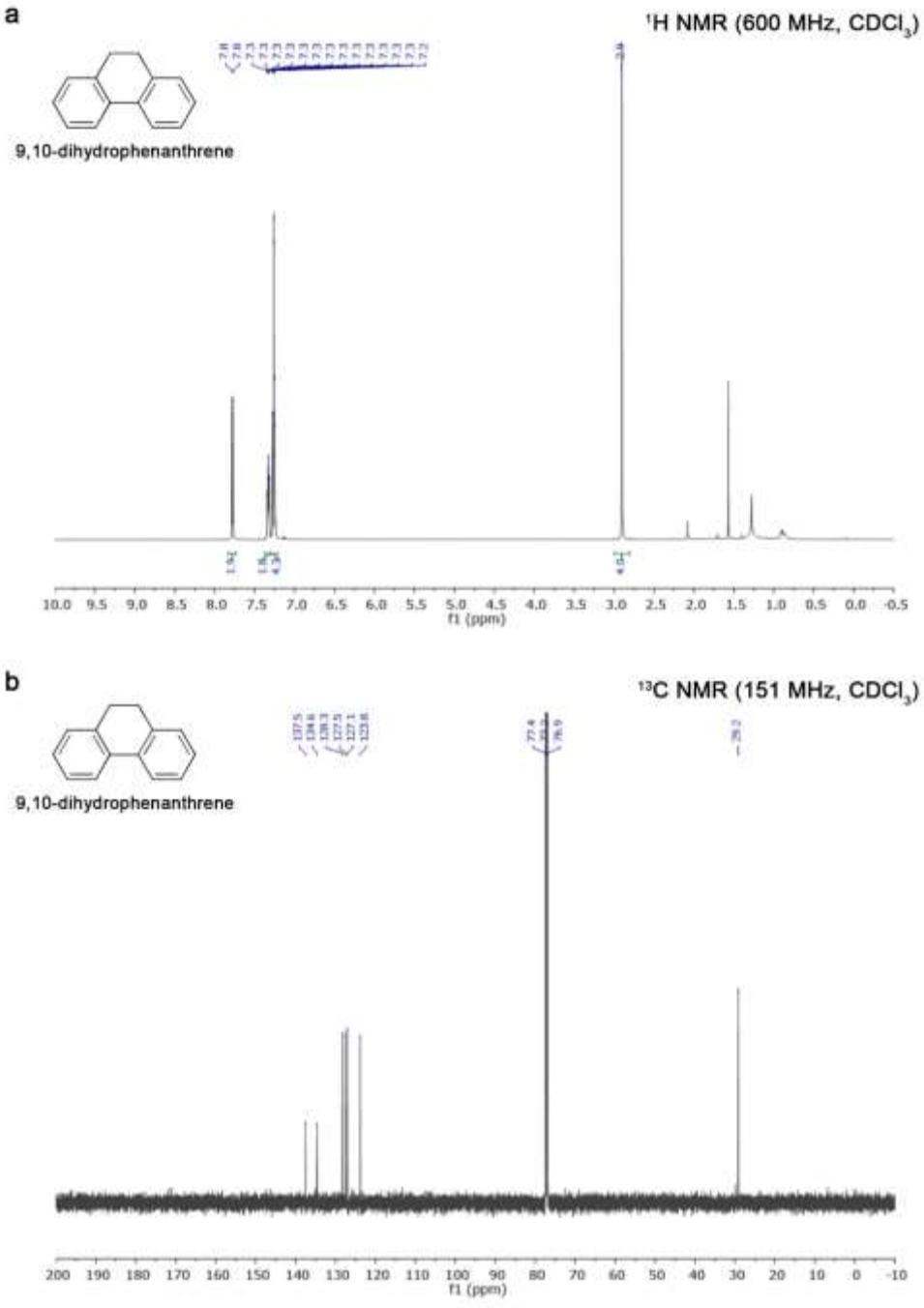

Figure S15. (a) ^{1}H- and (b) ^{13}C-NMR spectra of 9,10-dihydrophenanthrene.

Supplementary Tables

Table S1. Sherwood (*Sh*), Reynolds (*Re*), and Schmidt (*Sc*) Numbers Previously Used to Derive k_mA_s - u Relationships for Porous Electrodes.

Porous electrodes	*Sh*	*Re*	*Sc*	k_mA_s
Carbon fiber[1,5]	$\frac{k_m d}{D}$	$\frac{ud}{\nu}$	$\frac{\nu}{D}$	$a^* A_s \left(\frac{D}{d}\right)\left(\frac{d}{\nu}\right)^b \left(\frac{\nu}{D}\right)^c \boldsymbol{u^b}$
Iron felt[4]	$\frac{k_m A_s d^2}{D}$	$\frac{ud_H}{\nu}$ $\frac{ud}{\varepsilon\nu}$	$\frac{\nu}{D}$	$a^* \frac{D}{d^2}\left(\frac{d_H}{\nu}\right)^b \left(\frac{\nu}{D}\right)^c \boldsymbol{u^b}$ $a^* \frac{D}{d^2}\left(\frac{d}{\varepsilon\nu}\right)^b \left(\frac{\nu}{D}\right)^c \boldsymbol{u^b}$
Disordered fibrous 3D structure[6]	-	$\frac{\rho U_0}{(1-\varepsilon)A_s\mu}$	-	-
Fiber filter[5]	$\frac{k_m}{A_s D}$	$\frac{u}{A_s\nu}$	$\frac{\nu}{D}$	$a^* A_s^2 D \left(\frac{1}{A_s\nu}\right)^b \left(\frac{\nu}{D}\right)^c \boldsymbol{u^b}$

u: superficial velocity, d: fiber diameter, ν: kinematic viscosity, k_m: mass transfer coefficient, D: diffusion coefficient, d_H: hydraulic diameter, ε: porosity, A_s: specific surface area, ρ: density, U_0: volume-averaged superficial velocity, μ: viscosity.

Table S2. Relationship Between k_mA_s and u for Various Porous Electrodes.[8,9]

Flow-Through Electrodes	The Relationship between k_mA_s and u
Carbon Felt	$k_mA_s = 1.44\,u^{0.48}$
Ni Foam	$k_mA_s = 0.414\,u^{0.46}$
Steel Wool	$k_mA_s = 0.210\,u^{0.47}$
Reticulated Vitreous Carbon (RVC), 100 ppi[a]	$k_mA_s = 0.063\,u^{0.48}$
RVC, 60 ppi	$k_mA_s = 0.030\,u^{0.48}$
Perforated Carbon Paper	$k_mA_s = 0.0023\,u^{0.48}$
Cu Nanowire Felt (this study)	$k_mA_s = 36.5\,u^{0.77}$
Carbon Paper (this study)	$k_mA_s = 0.51\,u^{0.36}$

[a]ppi: pores per inch

Table S3. Physical Properties of Carbon Paper, Graphite Felt, Reticulated Vitreous Carbon (RVC), Ni Foam, and Cu Nanowire Felt.

	Carbon Paper[10–12]	Graphite Felt[13]	RVC[14–16]	Ni Foam[17]	Cu NW Felt (this study)
Resistivity (μΩ·cm)	$4.7–5.8\times10^{3}$	3×10^{5}	$2.3–6.9\times10^{5}$	1×10^{3}	143 (± 8)
Specific Surface Area (cm^2/cm^3)	1.6×10^{3}	2.3×10^{2}	$1.35–6.75\times10^{1}$	$1.9–4.1\times10^{2}$	2.4×10^{4} ($\pm 1.2\times10^{3}$)
Porosity (%)	78–80	98	90–97	97–98	94 (± 0.7)
Permeability (m^2)	10^{-12}	$10^{-10}–10^{-11}$	$10^{-9}–10^{-10}$	$1.8\times10^{-8}–2.6\times10^{-9}$	9.92×10^{-14} ($\pm 4.5\times10^{-15}$)

Table S4. Charge Transfer-Limited Currents (i_K) for Cu Ion Reduction and ARS Reduction over Cu Nanowire Felt and Carbon Paper.

		Cu Nanowire Felt	Carbon Paper
$CuSO_4$	**0.1 mM**	-25.48 mA	-8.07 mA
	1 mM	-28.23 mA	-10.04 mA
	10 mM	-29.99 mA	-16.23 mA
ARS	**1 mM**	-102.07 mA	-16.92 mA

References

(1) Schmal, D.; Van Erkel, J.; Van Duin, P. J. Mass Transfer at Carbon Fibre Electrodes. *J. Appl. Electrochem.* **1986**, *16*, 422–430.

(2) Delanghe, B.; Tellier, S.; Astruc, M. Mass Transfer to a Carbon or Graphite Felt Electrode. *Electrochim. Acta* **1990**, *35*, 1369–1376.

(3) Arenas, L. F.; Ponce de León, C.; Walsh, F. C. Engineering Aspects of the Design, Construction and Performance of Modular Redox Flow Batteries for Energy Storage. *J. Energy Storage* **2017**, *11*, 119–153.

(4) Lizarraga, D. S.; Bisang, J. M. Mass Transfer Studies at Iron Felts. *J. Appl. Electrochem.* **1996**, *26*, 1209–1215.

(5) Reichelt, E.; Heddrich, M. P.; Jahn, M.; Michaelis, A. Fiber Based Structured Materials for Catalytic Applications. *Appl. Catal. A* **2014**, *476*, 78–90.

(6) Rezk, K.; Forsberg, J.; Nilsson, L.; Berghel, J. Characterizing Flow Resistance in 3-Dimensional Disordered Fibrous Structures Based on Forchheimer Coefficients for a Wide Range of Reynolds Numbers. *Appl. Math. Model.* **2016**, *40*, 8898–8911.

(7) Nam, J. H.; Kaviany, M. Effective Diffusivity and Water-Saturation Distribution in Single- and Two-Layer PEMFC Diffusion Medium. *Int. J. Heat Mass Transf.* **2003**, *46*, 4595–4611.

(8) Walsh, F. C. *A First Course in Electrochemical Engineering*; The Electrochemical Consultancy: Romsey, U.K., 1993; pp 113–170.

(9) Arenas, L. F.; Ponce de León, C.; Walsh, F. C. 3D-Printed Porous Electrodes for Advanced Electrochemical Flow Reactors: A Ni/Stainless Steel Electrode and Its Mass Transport Characteristics. *Electrochem. Commun.* **2017**, *77*, 133–137.

(10) Hopkins, B. J.; Smith, K. C.; Slocum, A. H.; Chiang, Y.-M. Component-Cost and Performance Based Comparison of Flow and Static Batteries. *J. Power Sources* **2015**, *293*, 1032–1038.

(11) Barton, S. C.; Sun, Y.; Chandra, B.; White, S.; Hone, J. Mediated Enzyme Electrodes with Combined Micro- and Nanoscale Supports. *Electrochem. Solid-State Lett.* **2007**, *10*, B96–B100.

(12) Kjeang, E.; Michel, R.; Harrington, D. A.; Djilali, N.; Sinton, D. A Microfluidic Fuel Cell with Flow-Through Porous Electrodes. *J. Am. Chem. Soc.* **2008**, *130*, 4000–4006.

(13) González-García, J.; Bonete, P.; Expósito, E.; Montiel, V.; Aldaza, A.; Torregrosa-Maciáb, R. Characterization of a Carbon Felt Electrode: Structural and Physical Properties Experimental Details. *J. Mater. Chem.* **1999**, *9*, 419–426.

(14) Strohl, A. N.; Curran, D. J. Reticulated Vitreous Carbon Flow-Through Electrodes. *Anal. Chem.* **1979**, *51*, 353–357.

(15) Wang, J. Reticulated Vitreous Carbon-A New Versatile Electrode Material. *Electrochim. Acta* **1981**, *26*, 1721–1726.

(16) Walsh, F. C.; Arenas, L. F.; Ponce de León, C.; Reade, G. W.; Whyte, I.; Mellor, B. G. The Continued Development of Reticulated Vitreous Carbon as a Versatile Electrode Material: Structure, Properties and Applications. *Electrochim. Acta* **2016**, *215*, 566–591.

(17) Langlois, S.; Coeuret, F. Flow-Through and Flow-By Porous Electrodes of Nickel Foam. II. Diffusion-Convective Mass Transfer between the Electrolyte and the Foam. *J. Appl. Electrochem.* **1989**, *19*, 51–60.